IEEE Access
Multidisciplinary ⋮ Rapid Review ⋮ Open Access Journal

Received July 27, 2020, accepted August 14, 2020, date of publication August 26, 2020, date of current version September 9, 2020.

Digital Object Identifier 10.1109/ACCESS.2020.3019506

Efficient Estimation of the Helicopter Blade Parameter by Independent Component Analysis

INO CHOI[1], KI-BONG KANG[2], JOO-HO JUNG[3], AND SANG-HONG PARK[4]

[1]Agency for Defense Development, Chinhae 51678, South Korea
[2]Department of Electrical Engineering, Pohang University of Science and Technology, Pohang 37673, South Korea
[3]Department of Mechanical Engineering, Pohang University of Science and Technology, Pohang 37673, South Korea
[4]Department of Electronics Engineering, Pukyong National University, Busan 48513, South Korea

Corresponding author: Sang-Hong Park (radar@pknu.ac.kr)

This work was supported in part by the National Research Foundation of Korea (NRF) through the Basic Science Research Program funded by the Ministry of Education, Science, and Technology, under Grant 2018R1D1A1B07044981.

ABSTRACT We propose an efficient method to estimate various parameters of a helicopter blade including the number B_{num} and the length by separating the blade signal using independent component analysis (ICA) and an analytic solution obtained by monostatic/bistatic geometry. The proposed method is composed of two parts, one for even B_{num} and one for odd B_{num}. For even B_{num} the blade parameters are estimated using ICA plus analytic estimation. For odd B_{num} the parameters are estimated using two ICAs plus analytic estimation. Experimental results using the radar signal of a blade model calculated by physical optics demonstrate that the proposed method successfully separates the blade signals for both even and odd B_{num}s and estimates parameters with high accuracy.

INDEX TERMS Helicopter, micro-Doppler, ICA, radar target recognition, STFT.

I. INTRODUCTION

The helicopter is a major threat to radar and ground weapons in modern battlefield. By flying at a low altitude, a helicopter can avoid detection by radar. Therefore, methods must be developed to detect low-flying helicopters by using short- and medium range ground-based radar and sound signatures.

The rotating rotor of a helicopter generates a time-varying Doppler frequency, i.e., micro-Doppler (MD) frequency [1]–[3]. A conventional inverse synthetic aperture radar (ISAR) image may fail to classify the helicopter [4], [5] because the image is seriously blurred in the cross-range direction. In addition, processing to remove the MD signal from the rigid body signal can further degrade the quality of the image. However, the MD signal encodes the length l, the number B_{num} of blades, and various observation parameters. Therefore, the MD frequency itself can be used to classify the helicopter.

Various methods have been proposed to estimate helicopter parameter by using a signal model and a time-frequency (TF) transform. Some methods [6]–[9] estimate the rotation velocity ω of the rotor blades by using the periodicity of wavelet transform and short-time Fourier transform (STFT) of the received signal, but these methods do not provide l and B_{num} simultaneously. In addition, when l and ω are estimated simultaneously from the TF image of a monostatic radar signal, local minima caused by a combination of the aspect angle (especially the elevation), l and ω can provide wrong results. Some methods [10], [11] assume that the blade flash, i.e., the high specular return from the blade, occurs along with the maximum Doppler frequency, and that the blade signal has relatively small amplitudes, then estimate l and B_{num} by using tomographic imaging [12] of the blade tip. However, the blade signal is very small compared with the maximum Doppler frequency due to the sharp decrease of the radar cross-section (RCS) of the rod-type blade; also, the equation used may yield many wrong results when it considers radar signals at various elevation angles.

Another method [13] assumes an ideal point scatterer and successfully estimates l, ω, and monostatic/bistatic angles by using the Hough transform cube (HTC) of the TF image of signals obtained from monostatic and bistatic measurement scenarios. However, this method is based on the assumption that the isotropic scatterer is perfectly separated and detected in HTC, so this method can yield a poor result when peaks in the Hough transform of the TF image are obscured by blade flashes. One method finds l and B_{num} by using the quotient L/N $= l/B_{num}$ [14], but this technique can also

The associate editor coordinating the review of this manuscript and approving it for publication was Jenny Mahoney.

produce wrong results because different helicopters can have the same L/N. A recently proposed method uses a maximum-likelihood estimator and information theoretic criteria to estimate l and B_{num} without ambiguity [15]. However, this paper did not consider variation in observation angle, and thus may yield wrong results because different radar signals observed at different elevation angles can have the same Doppler frequency.

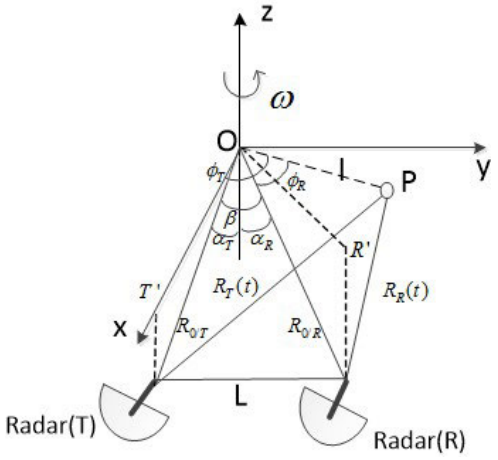

FIGURE 1. Monostatic/bistatic geometry for observing a point scatterer. Components and processes are described in the text.

This paper proposes an efficient method to estimate l, B_{num}, and various observation parameters by using independent component analysis (ICA) which has been proven to be a good method for signal separation in MD parameter estimation [16]. Using the blade flashes of the blade separated by ICA in monostatic/bistatic observation scenarios, the proposed method successfully reconstructs the sinusoidal time-varying frequency signal of each blade and thus successfully estimates l and ω. In addition, B_{num} is correctly estimated by using the characteristics of blade flash for each B_{num}.

Compared with existing methods, the proposed method prevents wrong results caused by an erroneous combination of l, B_{num}, and the elevation angle [6]–[9], [14], [15]. In addition, the proposed method does not require any complicated tomographic imaging, and prevents errors caused by the limited resolution of the Radon transform [10]–[12]. Furthermore, the proposed method utilizes the separated signal of each blade, and therefore can prevent enormous error caused by using the unseparated signal [13]. In simulations using the radar signal of a blade estimated by the method of physical optics (PO), the proposed method accurately estimated the blade parameters.

II. PROPOSED METHOD

A. ANALYTIC SOLUTION TO OBTAIN THE BLADE PARAMETERS

The proposed method uses the method proposed in [13] because it provides an analytic solution for l, ω, and various geometrical parameters by using a combination of monostatic and bistatic observations. The analysis considers a point scatterer P located at a distance l from the origin O and rotating at ω around the z axis, i.e., on the x-y plane, that is illuminated by radar T from a distance $R_T(t)$ at time t (Fig. 1). The received monostatic signals S_T at T and bistatic signal S_B at R at time t are

$$S_T(t) = \exp\left(-j2\pi \frac{2R_T(t)}{\lambda}\right), \tag{1}$$

$$S_B(t) = \exp\left(-j2\pi \frac{2R(t)}{\lambda}\right), \tag{2}$$

where λ is the wavelength of the radar signal, $R(t) = R_T(t) + R_R(t)$, and $R_R(t)$ is a distance to P from radar R. Similarly, assuming that radar R illuminates the target virtually, the received monostatic signal at R is

$$S_R(t) = \exp\left(-j2\pi \frac{2R_R(t)}{\lambda}\right). \tag{3}$$

Then differentiating (1) - (3) yields the corresponding MDs

$$f_T(t) = l_T \sin(\omega t + \phi_T), \tag{4}$$

$$f_B(t) = l_B \sin(\omega t + \phi_B), \tag{5}$$

$$f_R(t) = l_R \sin(\omega t + \phi_R), \tag{6}$$

where

$$l_T = -\frac{\omega}{\lambda} 2l \sin\alpha_T, \quad l_R = -\frac{\omega}{\lambda} 2l \sin\alpha_R, \; l_B = -\frac{\omega l A_B}{\lambda}. \tag{7}$$

A_B is given by

$$A_B = \sqrt{4\cos^2(\beta/2) - (\cos\alpha_R + \alpha_T)^2}, \tag{8}$$

where β is the bistatic angle, α_T is the angle between OT and the z axis, and α_R is the angle between OR and the z axis (Fig. 1).

The estimated amplitude, angular velocity, and initial phase of (4) - (5) by $(\hat{l}_T, \hat{\omega}, \hat{\phi}_T)$ and $(\hat{l}_B, \hat{\omega}, \hat{\phi}_B)$ respectively, can be found by analyzing the time-varying MD radar of the signals received at the radars T and R. $(\hat{l}_R, \hat{\phi}_R)$ can be calculated by using the following relationship [13]:

$$\hat{l}_R = \sqrt{\hat{l}_T^2 + 4\hat{l}_T\hat{l}_B \cos\left(\hat{\phi}_T - \hat{\phi}_B\right)}, \tag{9}$$

$$\hat{\phi}_R = \sin^{-1}\left(\frac{2\hat{l}_B \sin\hat{\phi}_B - \hat{l}_T \sin\hat{\phi}_T}{\hat{l}_R}\right). \tag{10}$$

Then, α_T, α_R and l are analytically calculated by

$$\hat{\alpha}_T = \sin^{-1}\left(\sqrt{\frac{-b \pm \sqrt{b^2 - 4ac}}{2a}}\right),$$

$$\hat{\alpha}_R = \sin^{-1}\left(\frac{B}{A}\sin\hat{\alpha}_T\right), \quad \hat{l} = \frac{A}{\sin\hat{\alpha}_T}, \tag{11}$$

where

$$a = \frac{B^2}{A^2}\left(1 - C^2\right), \quad b = \frac{2BC}{A}\cos\beta - 1, \; c = \sin^2\beta,$$

$$A = -\lambda\frac{\hat{l}_T}{2\hat{\omega}}, \quad B = -\lambda\frac{\hat{l}_R}{2\hat{\omega}}, \text{ and } C = \cos(\hat{\phi}_T - \hat{\phi}_R). \tag{12}$$

When the helicopter moves with a velocity v_0 and an acceleration a_0, the estimation results may be inaccurate because additional Doppler frequencies are added to (4) - (6). In this case, the phase caused by the Doppler frequency should be subtracted by multiplying (1) - (3) by $\exp(j4\pi R_a(t)/\lambda)$, where $R_a(t) = v_0 t + 0.5 a_0 t^2$. In this paper, we assume that the effect of $R_a(t)$ is perfectly removed by Doppler centroid tracking of the radar.

B. SEPARATION OF RADAR SIGNALS OF EACH BLADE BY USING INDEPENDENT COMPONENT ANALYSIS

The analytic method (section II.A) assumes that a complete signal from a scattering center, i.e., a blade, is obtained, but that radar signals from other blades overlap in the received signal. As a result, the analytical method can fail to estimate the parameters because of poor estimation of l and φ in (4) - (6). In this paper, we use ICA to distinguish the radar signals from each blade.

ICA is a widely used method to separate blind sources that are stochastically independent. The N complex random variables $\mathbf{x}(t) = [x_1(t)\, x_2(t)\, \ldots\, x_N(t)]^T$ received at N channels at t are combinations of the signals from N independent sources and can be given by

$$\mathbf{x}(t) = \mathbf{A}\mathbf{s}(t), \tag{13}$$

where $\mathbf{s}(t) = [s_1(t)\, s_2(t)\, \ldots\, s_N(t)]^T$ is a complex vector containing the signal from N blind sources and $\mathbf{A}$ is an $N \times N$ mixing matrix. $s_n(t)$ is the signal from blade n and $x_n(t)$ is that received at antenna n. The complex ICA finds the $N \times N$ separating matrix $\mathbf{W}$ that maximizes the non-Gaussianity, i.e., the independence, of the separated signals in $\mathbf{y}(t) = \mathbf{W}^H\mathbf{x}(t) \approx \mathbf{s}(t)$, where the superscript H is the complex conjugate.

Estimation of $\mathbf{W}$ can be inaccurate if $x_1(t), x_2(t), \ldots x_N(t)$ are correlated; therefore, centering and whitening are conducted as preprocessing to simplify the task of finding $\mathbf{W}$. Centering is simply subtraction of $m = E\{\mathbf{x}\}$ from $\mathbf{x}$ to make $\mathbf{x}$ zero-mean, where $E\{\}$ is the expectation operation using all time samples. Whitening transforms $\mathbf{x}$ to $\tilde{\mathbf{x}}$ with uncorrelated elements. Whitening can be completed simply by eigen-value decomposition of the covariance $E\{\mathbf{x}\mathbf{x}^H\} = \mathbf{E}\mathbf{D}\mathbf{E}^H$, where $\mathbf{E}$ is the matrix with eigenvectors of the covariance matrix and $\mathbf{D}$ is a diagonal matrix with corresponding eigenvalues. The whitened vector $\tilde{\mathbf{x}}$ is then written as

$$\tilde{\mathbf{x}} = \mathbf{E}\mathbf{D}^{-1/2}\mathbf{E}^H\mathbf{x}. \tag{14}$$

The non-Gaussian measure widely used is the entropy of the probability density function (pdf) of the random variable, and the entropy of the random vector $\tilde{\mathbf{y}} = \mathbf{w}^H\tilde{x}$, where $\mathbf{w}$ is a column vector of $\mathbf{W}$, composed of random variables with zero mean and fixed variances is defined as

$$H(\tilde{\mathbf{y}}) = -\int f(\tilde{\mathbf{y}}) \log(f(\tilde{\mathbf{y}}))d\tilde{\mathbf{y}}, \tag{15}$$

where $f(\tilde{\mathbf{y}})$ is the pdf of $\tilde{\mathbf{y}}$ [17], [18]. According to the information theory, a Gaussian variable has the largest entropy among random variables that have the same variance [17], [18]. Thus, $\mathbf{W}$ that maximizes the non-Gaussianity can be found by maximizing the negentropy, which is the entropy difference between the Gaussian random variables $\tilde{\mathbf{y}}_{gauss}$ and $\tilde{\mathbf{y}}$ that have the same covariance matrix, and that is defined as

$$J(\tilde{\mathbf{y}}) = H(\tilde{\mathbf{y}}_{gauss}) - H(\tilde{\mathbf{y}}). \tag{16}$$

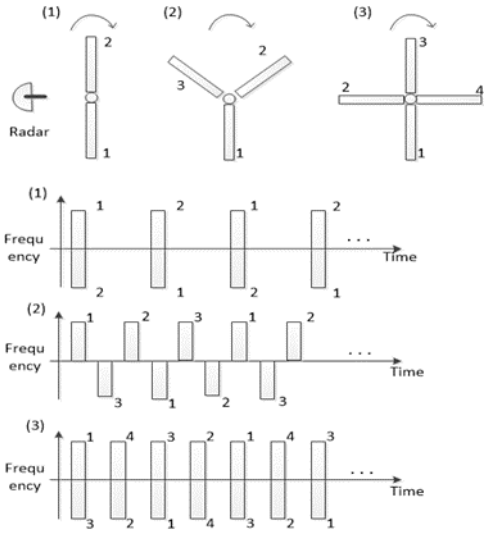

FIGURE 2. B_{num} and blade flashes.

Estimation of the parameters of the pdf is a difficult task, so a fixed point algorithm maximizes the well-defined contrast function given by

$$J_G(\mathbf{w}) = E\left\{G\left(\left|\mathbf{w}^H\tilde{\mathbf{x}}\right|^2\right)\right\}, \tag{17}$$

where $G(x)$ can be one of the following functions [19]:

$$G_1(x) = \sqrt{a_1 + x}, \quad G_2(x) = \frac{1}{2}x^2. \tag{18}$$

Maximization of (17) is identical to maximization of the negentropy [18]. Updating $\mathbf{w}$ to a new vector $\mathbf{w}_{\mathbf{new}}$ is direct and conducted by using the following rule [19]:

$$\begin{aligned}\mathbf{w}_{new} &= E\left\{\tilde{\mathbf{x}}\left(\mathbf{w}^H\tilde{\mathbf{x}}\right)^* g\left(\left|\mathbf{w}^H\tilde{\mathbf{x}}\right|^2\right)\right\} \\ &\quad - E\left\{g\left(\left|\mathbf{w}^H\tilde{\mathbf{x}}\right|^2\right) + \left|\mathbf{w}^H\tilde{\mathbf{x}}\right|^2 g'\left(\left|\mathbf{w}^H\tilde{\mathbf{x}}\right|^2\right)\right\}\mathbf{w}, \\ \mathbf{w}_{new} &= \frac{\mathbf{w}_{new}}{\|\mathbf{w}_{new}\|},\end{aligned} \tag{19}$$

where $g(x)$ and $g'(x)$ are respectively the first and the second derivatives of (20) and $*$ is the complex conjugate. Then to prevent convergence of all $\mathbf{w}$s to a vector that yields the same maximum negentropy, all columns are decorrelated by using the Gram-Schmidt-like decorrelation [19].

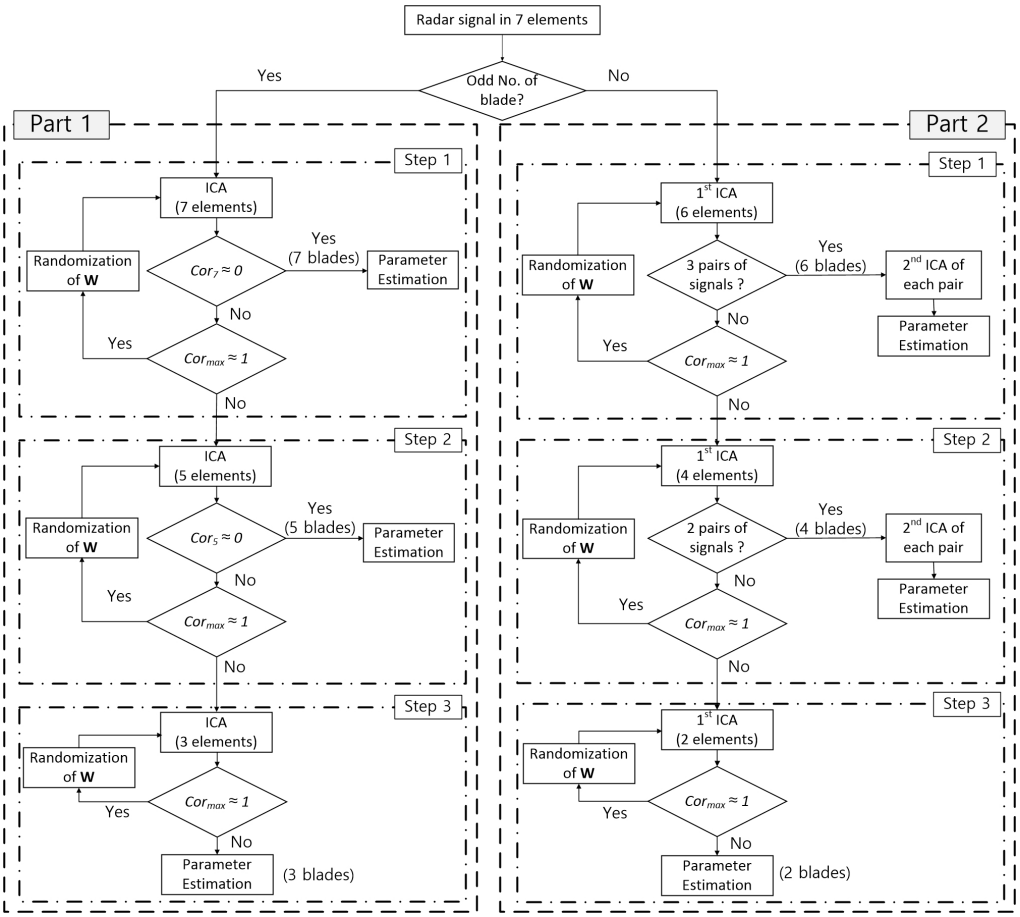

FIGURE 3. Overall procedure to estimate blade parameters. Components and processes are described in the text.

C. LOCAL MAXIMA PROBLEM FOR THE EVEN B_{num}

ICA separates unknown sources by maximizing non- Gaussianity. If signals from two sources such as the flashes from two blades occur at the same time, they can be easily separated by ICA by maximizing the non-Gaussianity of each signal (Fig. 2). In addition, if the signals from the sources do not occur at the same time, ICA can separate the signals easily because they do not interfere with each other. Therefore, separation of the radar signal from a helicopter with odd B_{num} such as 3 (Fig. 2), 5, or 7 is an easy task once the number of antenna elements has been matched to the number of sources.

However, for a helicopter that has even B_{num}, two blade flashes, one with positive frequency and one with negative frequency, can occur simultaneously. For example, in the received signal from a four-blade helicopter, two sets of the simultaneous positive and negative blade flashes, i.e., the blade flashes of the blade 1 and 3 and those of the blade 2 and 4, occur alternately (Fig 2). In this case, the ICA algorithm separates the blades by obtaining the maximum of (17), but a local maximum can occur, in which two sets of signals, a sum of signals from blades 1 from 3 and the other from blades 2 and 4, are separated; according to the central limit theorem [20], this condition is inevitable because a sum of two signals is more Gaussian than a single independent signal and less Gaussian than a sum of other even numbers of signals.

This local maximum is near the global maximum, so the ICA algorithm that uses a fixed point-gradient always stops at this local maximum, and yields an independent sum of signals from blades 1 and 3 in each of two channels and another independent sum of signals from blades 2 and 4 in each of the other two channels. Therefore, another ICA must be applied that uses the two-channel signals from the same blades to separate the blade signals from blades 1 and 3, and those from 2 and 4. In the case of six blades, three independent sums of signals, one from 1 and 4, another from 2 and 5, and the other from 3 and 6, are obtained in each of two-channels.

D. PROPOSED PARAMETER ESTIMATION METHOD

Assuming that a phase array antenna composed of at least seven elements (= channels in (13)) is used for general $2 \leq B_{num} \leq 7$, the proposed parameter estimation method is composed of two parts, one for odd-numbered blades and the other for even-numbered ones, and each part is composed of three steps. Both of the two parts estimate the parameter starting from the largest number of B_{num} to the smallest one,

i.e., 7 (step 1) → 5 (step 2) → 3 (step 3) in part 1 and 6 (step 1) → 4 (step 2) → 2 (step 3) in part 2, until the condition for each B_{num} is met (Fig. 3).

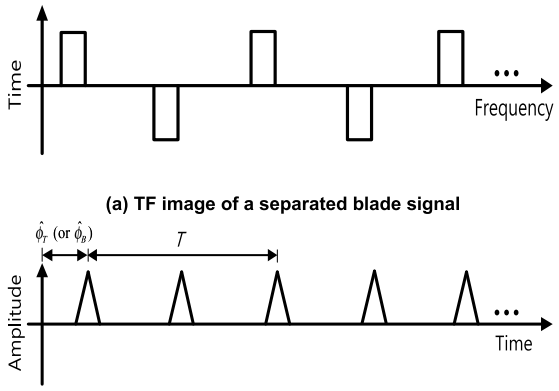

FIGURE 4. TF image and 1D amplitude distribution of a separated blade signal in time.

Once the radar signal composed of the blade signals from an unknown B_{num} is received by seven elements, the first test determines whether B_{num} is even or odd. This can be easily done by checking whether positive-frequency and negative-frequency flashes occur alternately or simultaneously. If B_{num} is odd, the three steps in part 1 are conducted to determine whether $B_{num} = 7$, 5, or 3. This estimation of odd B_{num} is a very easy condition, so the signals can be easily separated once the number of antenna elements is equal to B_{num}. In a similar manner, if B_{num} is even, three steps in part 2 are conducted to determine whether $B_{num} = 6, 4$, or 2. The difference is that another ICA is applied to separate blade signals simultaneously occurring (Fig. 2). The parts are described in the next sections.

The computation speed of the proposed method is dependent on that of the fast ICA. Negentropy obviously converges to the global maximum and the CPU cost of fast ICA is $O(2i_t i_c(i_c+1)N_s)$, where i_t is the number of the iteration, i_c is the dimension (= number of channels), and N_s is the number of samples [21]. In the proposed method, the maximum i_c is seven and the fast ICA converges to the global minimum for $5 \leq i_t \leq 10$, so i_c and i_t can be regarded as fixed coefficients. Therefore, the CPU complexity of the proposed method is $O(N_s)$, which provides real-time computation.

1) ALGORITHM PART 1

If $B_{num} = 7$, then ICA using signals in seven elements yields seven independent signals with each blade flash occurring at different time in step 1 of part 1. This can be found by checking the correlation Cor_7 of the seven binary TF images (TFBs), each of which is constructed by

$$TFB[i,j] = \begin{cases} 1, & \text{if } TF[i,j] > m\_p \times th \\ 0, & \text{otherwise,} \end{cases} \quad (20)$$

where TF is a TF image, m_p is the maximum pixel value of TF, and $0.4 \leq th \leq 0.6$ is an appropriate threshold ratio.

Pixels in TF that have near-zero frequency have large amplitudes due to the scattering centers near the rotor shaft and the rigid body, so the TFBs can be strongly correlated.

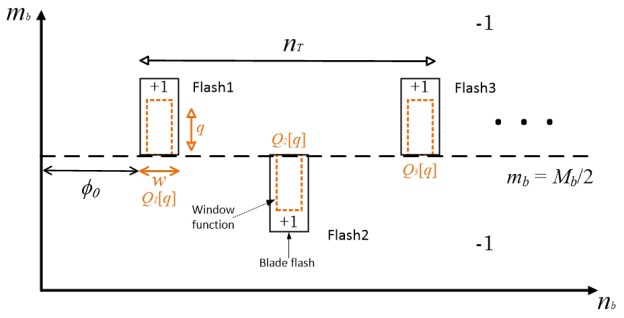

FIGURE 5. Window function $Q_i[q]$ to estimate $\hat{l}_T$ (or $\hat{l}_B$).

Therefore, '1' values in the TFB are set to '0' for low frequencies between f_{min} and f_{max}. Then, each TFB is normalized by the square root of the sum of binary pixels, and Cor_7 of the normalized TFBs (TFBNs) are given by

$$Cor_7 = \sum_{i=1}^{6} \sum_{j=i}^{7} \sum_{m_b=1}^{M_b} \sum_{n_b=1}^{N_b} TFBN_i \circ TFBN_j[m_b, n_b], \quad (21)$$

where $TFBN_k$ is the M_b by N_b TFBN of the separated signal k and is the Hadarmard product. If each blade signal is completely separated, the blade flash of each blade occurs at a different time, so $Cor_7 \approx 0$; otherwise, $Cor_7 \gg 0$.

Once the blade signal is separated, parameters can be estimated by the analytic solution (subsection II. *A*). However, the existing methods use the Hough and Radon transforms, which require much computation time to find $(\hat{l}_T, \hat{\omega}, \hat{\phi}_T)$ and $(\hat{l}_B, \hat{\omega}, \hat{\phi}_B)$ because the transforms use many possible combinations [10], [13]; the Hough-transform-based method finds all possible combinations of the three parameters, and Radon transform utilizes all possible combinations of $(\hat{\omega}, \hat{\phi}_T)$ and $(\hat{\omega}, \hat{\phi}_B)$. In this paper, we propose a simple window-matching method that is faster and more accurate than these methods.

The proposed method first estimates $\hat{\omega}$, then finds $\hat{\phi}_T$ (or $\hat{\phi}_B$) and $\hat{l}_T$ (or $\hat{l}_B$) sequentially. For a given TF image of the separated signal of a blade (Fig. 4a), the one-dimensional (1D) amplitude distribution can be obtained by summing pixel values for all f at each time (Fig. 4b). Then $\hat{\omega}$ can be easily estimated by finding the time interval between the peak s and $s+2$ (Fig. 4b); this interval is the period T ($\omega = 2\pi/T$). In addition, $\hat{\phi}_T$ (or $\hat{\phi}_B$) can be found by a simple equation to express the first peak in 1D amplitude distribution in time. Let the time of the first blade flash be T_{p1}. If the sum S_{po} of the pixels for $f > 0$ at T_{p1} is larger than the sum S_{ne} of the pixels for $f < 0$, then the phase of the TF frequency is $\pi/2$;

otherwise it is $3\pi/2$. Thus, $\hat{\phi}_T$ (or $\hat{\phi}_B$) are

$$\hat{\phi}_T(\text{or } \hat{\phi}_B) = \begin{cases} \frac{\pi}{2} - \frac{2\pi}{T} T_{p1}, & \text{for } S_{po} > S_{ne} \\ \frac{3\pi}{2} - \frac{2\pi}{T} T_{p1}, & \text{for } S_{po} < S_{ne}. \end{cases} \quad (22)$$

$\hat{l}_T$ (or $\hat{l}_B$) can be found by finding the frequency extent of the TF image of the blade flash (Fig. 2). However, depending on the time of the flash, $\hat{l}_T$ (or $\hat{l}_B$) can be slightly different due to the RCS variation caused by the different aspect angle, because amplitude and time-duration vary over time so the horizontal and vertical extents of a blade differ on a TF image. In this paper, we use the total number of pixels contained in the blade flash of the TF image (Fig. 5). For this purpose, we construct the binary image $I[m_b, n_b]$; pixels that have a value larger than the average pixel value p_{av} in the TF image are set to 1, and the others to -1.

If the first flash has positive frequencies at $n_b = \varphi_0$, then $I[m_b, n_b]$ is multiplied by the following window function with a length q in m_b direction for every half period in n_b (Fig. 5):

$$\begin{aligned} &Q[m_b, n_b, i, q] \\ &= Q_i[q] \\ &= rect\left[\frac{n_b - ik_T/2 - \phi_0}{w}\right] \times \left(u\left[(-1)^{i-1}(m_b - M_b/2)\right]\right. \\ &\quad \left. - u\left[(-1)^{i-1}(m_b - M_b/2 - q)\right]\right), \end{aligned} \quad (23)$$

where $1 \le m_b \le M_b$, $1 \le n_b \le N_b$, and $1 \le i \le N_f$. N_f is the number of flashes, which is equal to the number of peaks in Fig. 4b and $k_T = T \times$ pulse repetition frequency (PRF) is the number of indices that correspond to T, and w is an appropriate range window that is determined by the width of blade flash. i-1 in (23) is changed to i when the first blade flash has negative frequencies. $\hat{l}_T$ (or $\hat{l}_B$) is q that maximizes

$$A(q) = \sum_{m_b} \sum_{n_b} \sum_{i} I[m_b, n_b] Q[m_b, n_b, i, q]. \quad (24)$$

$A(q)$ increases in proportion to q until all of blade flash pixels ($I[m_b, n_b] = 1$) are included in (23), and decreases when non-flash pixels ($I[m_b, n_b] = -1$) are included (Fig. 5). Finally, the obtained $(\hat{l}_T, \hat{\omega}, \hat{\phi}_T)$ and $(\hat{l}_B, \hat{\omega}, \hat{\phi}_B)$ are applied to the analytic solution in (9) - (11) to yield blade parameters.

However, if initial values of $\mathbf{W}$ are not properly set for $B_{num} = 7$, the gradient-based method may rarely provide a solution at a local maximum that yields unseparated TF images similar to those before ICA. In this case, Cor_7 becomes $\gg 0$ so $\mathbf{W}$ must be randomly reset to obtain separated signals. This step can be conducted by checking the maximum correlation Cor_{max} of the TFB of one signal before ICA with the TFBs of the separated signals after ICA; Cor_{max} is defined by

$$Cor_{\max} = \max\left\{\sum_{m_b=1}^{M_b} \sum_{n_b=1}^{N_b} TFBN' \circ TFBN_i[m_b, n_b]\right\} \quad \text{for } i = 1, 2, \ldots, 7, \quad (25)$$

where $TFBN'$ is the TFBN of one signal before ICA, obtained by (20) and low-frequency thresholding. $Cor_7 \gg 0$ and $Cor_{max} \approx 1$ mean the source signals were not separated, so ICA is conducted again by randomly resetting $\mathbf{W}$ until signals are completely separated (Step 1 of Part 1 in Fig. 3).

However, if $Cor_7 \gg 0$ and $Cor_{max} \ll 1$, the ICA separated the signals successfully, so the TFBN of the separated signal is very different from that of the signal before ICA, but signals from the same blade repeat. For example, if $B_{num} = 5$, ICA yields five independent signals but signals from the same blade can be repeated because B_{num} is smaller than the number of channels, so the analysis yields a large $Cor_7 \approx 2$. In addition, the blade signals are separated, so $Cor_{max} \ll 1$ and $\approx 1/5$ because the TF image after ICA had one blade signal, whereas the TF image before ICA had five blade signals. The result with $Cor_7 \gg 0$ and $Cor_{max} \ll 1$ can also occur for $B_{num} = 3$, so ICA using signals in five antenna elements are conducted and Cor_5 with $6 \to 4$ and $7 \to 5$ in (21) is tested to determine whether $B_{num} = 5$.

The value of Cor_5 determines the subsequent steps. $Cor_5 \approx 0$ means that signals are completely separated, so parameters are estimated using (9) - (11) and (22) - (24) (Step 2 of Part 1 in Fig. 3). If $Cor_5 \gg 0$, Cor_{max} is calculated by varying i from 1 to 5 in (25) to determine whether the large Cor_5 is due to unseparated signals or repeated signals of three blades. If $Cor_{max} \approx 1$, $\mathbf{W}$ is randomly set and step 2 is repeated. If $Cor_{max} \ll 1$ and $\approx 1/3$, the B_{num} is 3 and signals from the same elements repeat so step 3 is performed; ICA using the signals in three elements is conducted and Cor_{max} is tested using $1 \le i \le 3$ in (25). If $Cor_{max} \ll 1$, parameters are estimated using the same procedures as in steps 1 and 2; otherwise $\mathbf{W}$ is randomly reset and step 3 is repeated (Step 3 of Part 1 in Fig. 3).

2) ALGORITHM PART 2

The part 2 of the proposed method is to determine the even B and each step is composed of two ICAs due to the local maximum of the fixed-point algorithm (Part 2 in Fig. 3). In the first step, a test is conducted to determine whether $B_{num} = 6$. As mentioned in subsection II. C, three pairs of similar signals are obtained, one from blades 1-4, one from blades 2-5, and one from blades 3-6, so the presence of six blades can be confirmed by simply finding three pairs of similar signals. After the 1st ICA using signals in six elements, the existence of three pairs can be tested by using a 6×6 matrix composed of correlations of two TFBNs:

$$Mat_{cor}[i, j] = Round\left(\sum_{m_b=1}^{M_b} \sum_{n_b=1}^{N_b} TFBN_i \circ TFBN_j[m_b, n_b]\right), \quad (26)$$

where $Round()$ is a function that rounds elements of Mat_{cor} to the nearest integer, $TFBN_i$ and $TFBN_j$ are the ith and jth TFBNs as in (21). $Mat_{cor}[i, j] = 1$ for $i = j$ and when TFBN i and j are a pair; therefore the sum of all elements in Mat_{cor} is 12 if three pairs exist. Then the second ICA is applied

to each pair to separate the two signals. Finally, parameters are estimated by applying the same procedure as for the odd B_{num}s by using (9) - (11) and (22) - (24) (Step 1 of Part 2 in Fig. 3).

If three pairs are not found, then Cor_{max} is tested at $1 \leq i \leq 6$ in (25) to determine whether the result was caused by a poor initial value; if $Cor_{max} \approx 1$, $\mathbf{W}$ is randomly reset and step 1 of the part 2 is repeated, but if $Cor_{max} \ll 1$, which means that either $B_{num} = 4$ ($Cor_{max} \approx 1/4$) or $B_{num} = 2$($Cor_{max} \approx 1/2$), then the second step to determine whether $B_{num} = 4$ is conducted (Step 2 of Part 2 in Fig. 3). Similar to the first step, signals from four elements are applied to ICA, yielding four signals and a 4×4 Mat_{cor} calculated as in (26). If two pairs of signals are found by finding the element sum of $Mat_{cor} = 8$, then $B_{num} = 4$, and each pair is input to the second ICA to separate the signals from the four blades, and to estimate the parameters. If $B_{num} \neq 4$ and $Cor_{max} \approx 1$ with $1 \leq i \leq 4$ in (25), $\mathbf{W}$ is randomly reset and the step 2 of part 2 is repeated, but if $Cor_{max} \ll 0$ and $\approx 1/2$, then estimates the parameters of the two blades. Likewise, the test for local maxima using Cor_{max} is conducted with $i = 1$ and 2 to yield the completely-separated signals (Step 3 of Part 2 in Fig. 3).

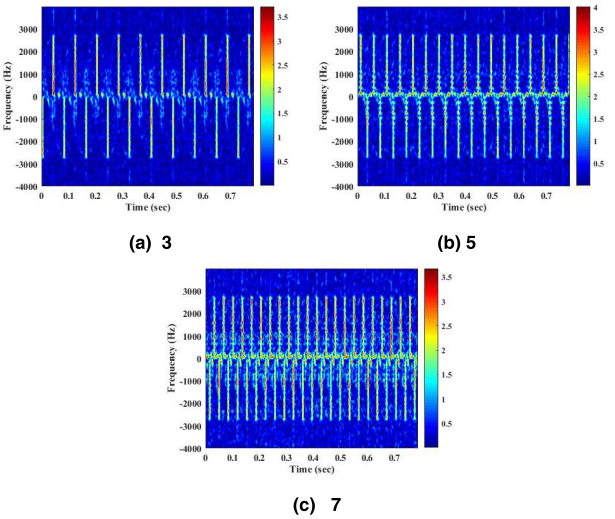

FIGURE 6. Blade flashes for odd B_{num}. Bistatic blade flashes omitted due to the similarity.

III. EXPERIMENTAL RESULT

A. EXPERIMENTAL CONDITION

To demonstrate the efficiency of the proposed method, the various types of propeller were modelled using a single blade with length $l = 5$ m, width $w_a = 0.3$ m, and height $h = 0.1$ m, which was composed of a perfect electrical conductor. The blade was assumed to rotate at $\omega = 26$ rad/s and to be observed by bistatic radars located at $(100, 0, -300)$ km and $(100, 20, -300)$ km, at aspect angles $\alpha_T = 71.57°$ and $\alpha_R = 71.23°$ respectively (Fig. 1). Physical optics (PO) was applied to obtain the complex reflected radar signal at frequency 10-GHz with a PRF = 8 kHz. $s(t)$ was obtained

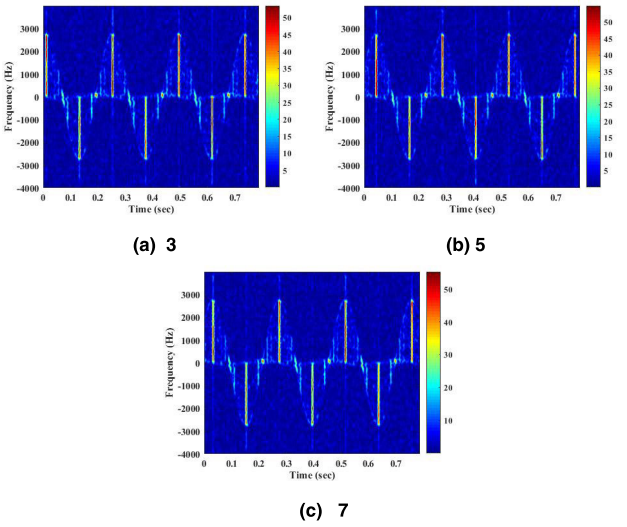

FIGURE 7. Separated blade signal for odd B_{num}. Only result of one blade is reported for each B_{num}, because the other blades showed similar results.

by positioning the received signal at the corresponding time delay; elements in $\mathbf{A}$ in (13) were chosen randomly from a uniform distribution from 0.5 and 1.

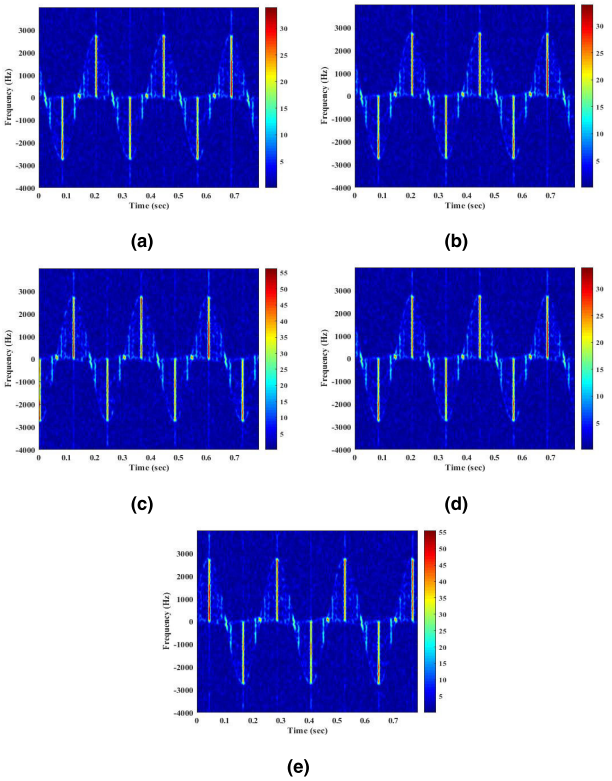

FIGURE 8. Repetition of blade flashes of one blade when ($B_{num} = 3$) < ($N = 5$). The signal in (a) repeats in (b) and (d).

To simulate the independent signals s_n(t) received by equally-spaced antenna elements $n = 1$ to N, the blade

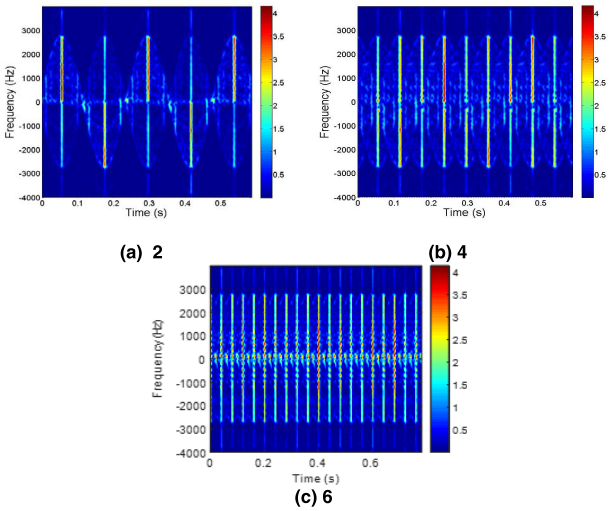

FIGURE 9. Blade flashes for even B_{num}. Bistatic blade flashes omitted due to the similarity.

was rotated in an increment of 0.1° from a certain rotation angle θ_r; for example, at $\theta_r = 5°$, seven elements received signals at angles 5.0°, 5.1°, 5.2°, . . . , 5.6°. Then, for the blade-flash analysis, the received signal was transformed to the TF domain by using the simple STFT [22]. The value of th was set to 0.4 to obtain TFB in (20) and to obtain TFBN in (21), f_{min} was set to -200 Hz and f_{max} was set to 200 Hz. w in (23) was set to 10. The signal to noise ratio was varied from 0 to 30 dB in increments of 5 dB.

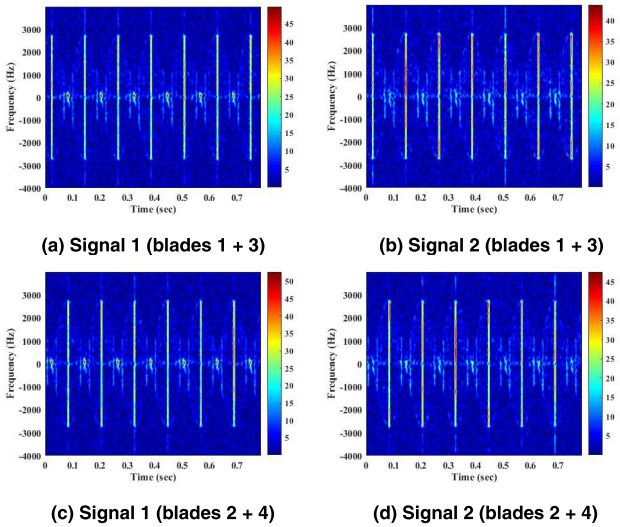

FIGURE 10. Result of the 1st ICA ($B_{num} = 4$).

B. SEPARATION RESULT

Blade flashes obtained at SNR = 10 dB appear alternately for odd B_{num} 3, 5, or 7 (Fig. 6). These three types of propeller have the same TF pattern except that the time interval between positive and negative flashes decreases as the

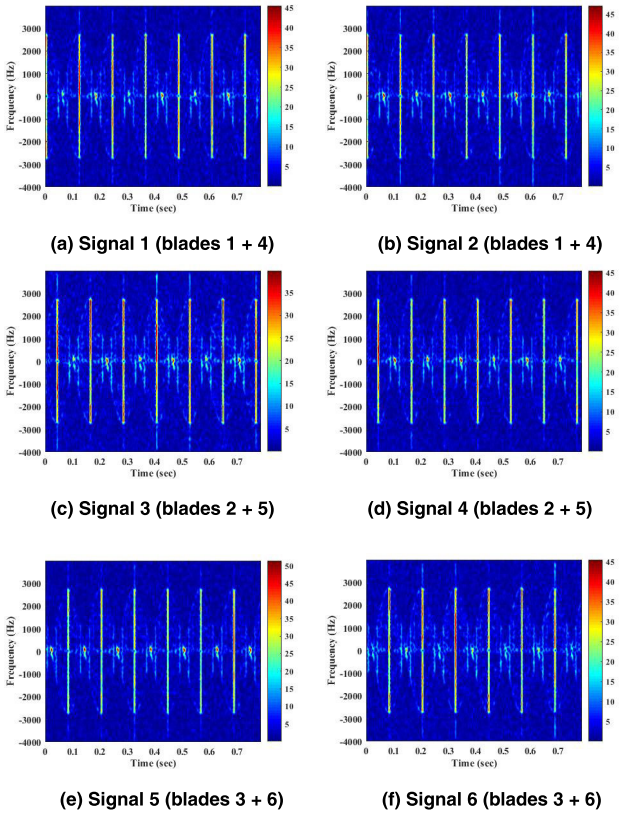

FIGURE 11. Result of the 1st ICA ($B_{num} = 6$).

number of blade increases. Separation using the part 1 of the proposed method is easy because blade flashes appear at distinct times, so the blade signals are completely separated by ICA when the number of the antenna elements $N = B_{num}$ (Figs. 6, 7). A blade signal repeats in the two channels when $(B_{num} = 3) < (N = 5)$, and yields a large $Cor_5 = 3.55$ (Fig. 8a-e); three signals of one blade repeat (Fig.8a, b, d).

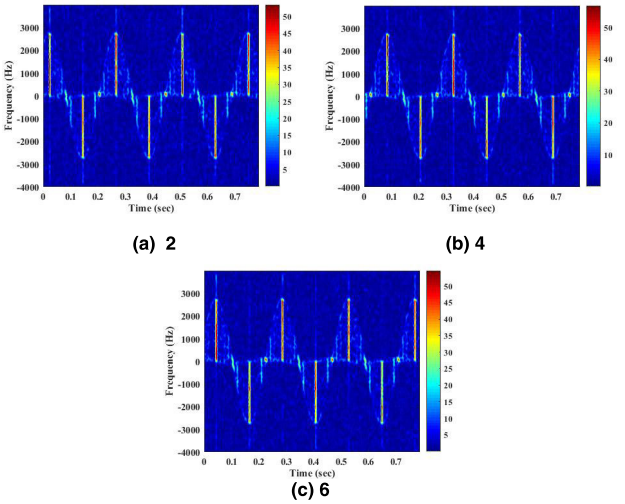

FIGURE 12. Separated blade signals for even B_{num}. For each B_{num}, separation result of a representative blade is shown because the other blades showed similar results.

For even $B_{num} = 2, 4$, or 6, the blade flashes were separated using part 2 of the proposed algorithm for SNR = 10 dB (Figs. 9 - 12). Due to the even numbers, positive and negative flashes occurred at the same time, with the flash interval decreasing as B_{num} increased (Fig. 9). When $B_{num} = 2$, the fixed-point fast ICA can successfully separate the signals from the two blades. However, ICA stopped at the local minimum and generated pairs of signals for $B_{num} = 4$ and 6 (Figs. 10, 11); for $B_{num} = 4$, ICA separated two signal pairs, one from blades 1 and 3 and one from blades 2 and 4 (Fig. 11), whereas for $B_{num} = 6$, ICA separated three signal pairs of signals, one from blades 1 and 4, one from blades 2 and 5, and one from blades 3 and 6 (Fig. 11). Therefore, application of each pair to the second ICA by grouping pairs using (26) separated the blade signal successfully by finding the global optimum in non-Gaussianity (Fig. 12).

C. ANALYSIS ON THE ESTIMATION ACCURACY FOR VARIOUS SNRS

Estimation accuracy on (22) - (24) (Figs. 4, 5) was first evaluated by using the separated flashes of $B_{num} = 3$ at SNR = 10 dB. Due to the complete separation of three blade signals, 1D amplitude distribution in time clearly shows peaks at each corresponding blade flash (Fig. 13a, b). The time interval between successive peaks was 0.1208 s, so the estimated T and $\hat{\omega}$ were 0.2417 s and 25.9994 rad/s, respectively. In addition, using at $T_{p1} = 0.04412$ s, $\hat{\phi}_T$ obtained using (22) was 3.5655 rad, and $\hat{l}_T$ obtained using the peak of the cost function (24) was 2.7885 kHz. In the same manner, the bistatic estimation result $(\hat{\phi}_B, \hat{l}_B)$ was (3.6626, 2.7924 kHz) (figures not shown due to similarity with the monostatic case).

TABLE 1. Estimation result of each parameters ($B = 3$).

Parameter	Theoretical value	Estimated value	Error [%]
$\hat{l}_T$	2739.93 Hz	2776.7 Hz	1.324 %
$\hat{l}_B$	2788.673 Hz	2784.6 Hz	0.146 %
$\hat{l}_R$	2863.5 Hz	2818.6 Hz	1.593 %
$\hat{\phi}_T$ - $\hat{\phi}_B$	0.09861 rad	0.09710 rad	1.555 %
$\hat{\alpha}_T$	1.2491 rad	1.2417 rad	0.596 %
$\hat{\alpha}_B$	1.2432 rad	1.2365 rad	0.542 %
$\hat{l}$	5 m	4.9554 m	0.900 %
$\hat{\omega}$	26 rad/s	25.9994 rad/s	0.002 %

Using $(\hat{\phi}_T, \hat{l}_T)$ and $(\hat{\phi}_B, \hat{l}_B)$, the analytic solution in II. *A* yielded very accurate estimation results (Table 1). $\hat{\omega}$ was very accurately estimated with 0.015 % error, and $(\hat{\phi}_T, \hat{l}_T)$ and $(\hat{\phi}_B, \hat{l}_B)$ were estimated with errors < 1.6 %. These errors were caused by the window overlap during calculation of the TF image, and by the RCS variation of the blade. The 'Spectrogram' function of MATLAB divides the signal into eight segments that overlap by 50%, so this process inevitably causes error in $\hat{\phi}_T$ and $\hat{\phi}_B$. Wigner-Ville-based high-resolution TF methods can reduce the error significantly but we did not use them because they would increase the computation time. RCS variation of the blade caused different numbers of pixels for each flash in $I[m_b, n_b]$ yielding 1.324 % error in $\hat{l}_T$ and 0.146 % error in $\hat{l}_B$. As a result, the blade length l was estimated with error = 0.900 % (Table 1).

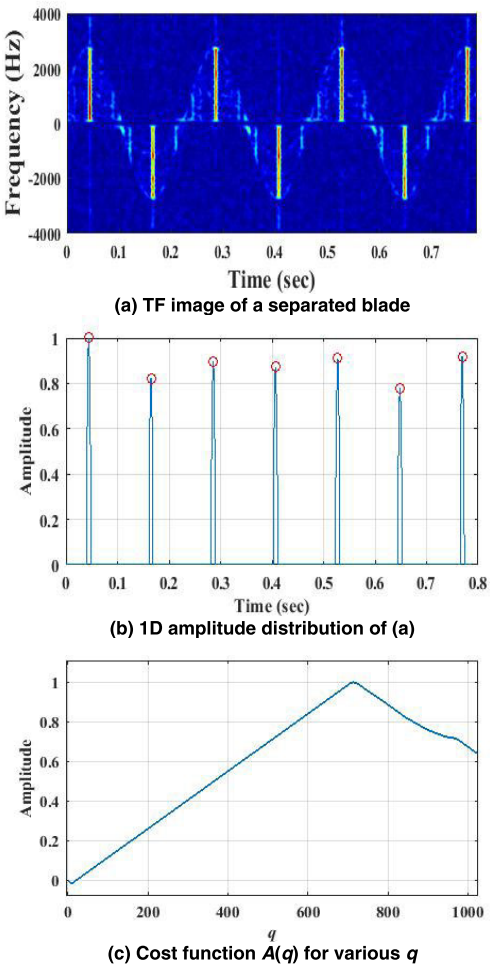

(a) TF image of a separated blade

(b) 1D amplitude distribution of (a)

(c) Cost function $A(q)$ for various q

FIGURE 13. TF image, 1D amplitude distribution, and $A(q)$ in (22) for various q ($B_{num} = 3$).

These evaluations were used to estimate the accuracy of parameters for various SNRs from 30 dB to 0 dB in decrements of 5 dB by adding white Gaussian noise; simulations were conducted 100 times for each blade number and the average error rate in percent with respect to the original value was used for analysis. Low estimation errors demonstrate the accuracy of the proposed method (Fig. 14). Errors generally decreased as SNR increased, but $\hat{l}$ was estimated within 2 % error (Fig. 14a); this is larger than the value in Table 1 for $B_{num} = 3$ because of errors caused while estimating other parameters.

The error was mainly caused by the relatively large error in $\hat{\phi}_T - \hat{\phi}_R = 0.09710$ rad, which determines C in (12) and all parameters in (9) - (11). This error occurs because of the slight change of the signal after ICA, the variation of RCS, and the

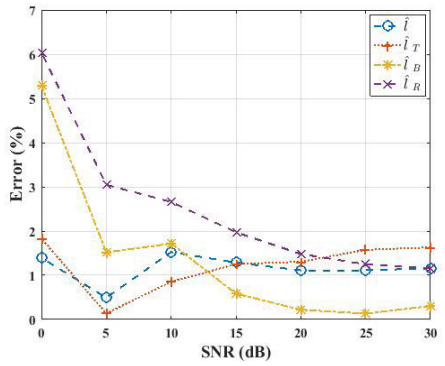

(a) $\hat{l}$, $\hat{l}_T$, $\hat{l}_B$, and $\hat{l}_R$

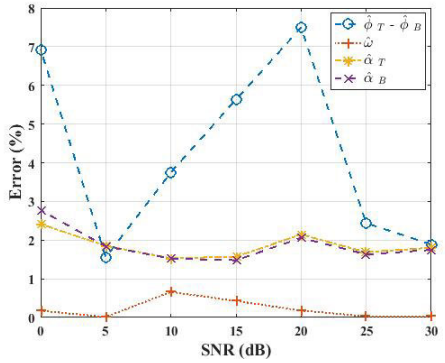

(b) $\hat{\phi}_T - \hat{\phi}_B$, $\hat{\alpha}_T$, $\hat{\alpha}_B$, and $\hat{\omega}$

FIGURE 14. Error rate for various SNRs.

time duration of the blade flash depending on B_{num}. ICA can be regarded as a filtering operation, so signals separated by ICA can be slightly changed, and this change can affect the shape of the TF image. For $B_{num} = 4$ and 6, two ICAs were used so the error was slightly larger than for $B_{num} = 2$, 3, 5, and 7. In addition, RCS change depending on the aspect angle and sampling timing changed TF image slightly. Time duration of the blade flash was also a factor of the error in $\hat{\phi}_T$-$\hat{\phi}_R$; as B_{num} increased, the duration of the blade flash decreased, so estimation errors in $\hat{\phi}_T$-$\hat{\phi}_R$ increased. Because of the low-resolution of the TF image and the small $\hat{\phi}_T$-$\hat{\phi}_R$, estimation errors corresponding to one or two indices were up to 10 % ($\approx 0.56°$).

The errors in $\hat{l}_T$ and $\hat{l}_B$ were caused by thresholding to obtain TFBs using (23); different shapes of TF yielded different TFBs after thresholding and this difference caused the errors. However, the percentage of error was negligible due to the large Doppler frequency of the blade flash. The error in $\hat{\omega}$ was very small because the error caused by the duration of the blade flash was negligible in the whole period T. The errors in $\hat{\alpha}_T$ and $\hat{\alpha}_R$ were caused by a combined influence of $\hat{l}_T, \hat{l}_B, \hat{\phi}_T$ - $\hat{\phi}_R$, and $\hat{\omega}$ in (12), so the errors were slightly larger than those of $\hat{l}_T, \hat{l}_B$. The slight difference was caused by the errors in $\hat{\phi}_T$ - $\hat{\phi}_R$.

IV. CONCLUSION

We have presented an efficient method to estimate B_{num}, l, and various observation parameters of the blade of a helicopter by using the independent component analysis and the analytic solution obtained from monostatic/bistatic geometry. Depending on the alternations of the blade flash in TF image, the proposed method is divided into two parts, one for odd B_{num} and one for even B_{num}. Each of these parts is composed of three steps to estimate the possibility of B_{num} in orders of $7 \rightarrow 5 \rightarrow 3$ for odd B_{num}, and $6 \rightarrow 4 \rightarrow 2$ for even B_{num} by using the correlation of TF image after using ICA to separate the radar signal. For odd B_{num}, blade flashes did not occur simultaneously so each blade signal was separated easily by applying ICA. However, even B_{num} required two ICAs because of the simultaneous blade flash by two blades; the first ICA separated $B_{num}/2$ pairs of the signal composed of sums of two signals generating blade flashes simultaneously and the second ICA separated two signals from each pair. Experimental results using the radar signal computed by PO for various B_{num} demonstrated that ICA successfully separated the blade signal, and that l, B_{num}, and various parameters were estimated accurately.

REFERENCES

[1] V. C. Chen, F. Li, S.-S. Ho, and H. Wechsler, "Micro-Doppler effect in radar: Phenomenon, model, and simulation study," *IEEE Trans. Aerosp. Electron. Syst.*, vol. 42, no. 1, pp. 2–21, Jan. 2006.
[2] G. E. Smith, K. Woodbridge, and C. J. Baker, "Micro-Doppler signature classification," in *Proc. CIE Int. Conf. Radar*, Oct. 2006, pp. 1–4.
[3] P. Pouliguen, L. Lucas, F. Muller, S. Quete, and C. Terret, "Calculation and analysis of electromagnetic scattering by helicopter rotating blades," *IEEE Trans. Antennas Propag.*, vol. 50, no. 10, pp. 1396–1408, Oct. 2002.
[4] C. Özdemiiïr, "Inverse synthetic aperture radar imaging and its basic concepts," in *Inverse Synthetic Aperture Radar Imaging with MATLAB Algorithms*. Hoboken, NJ, USA: Wiley, 2012.
[5] S.-J. Lee, S.-H. Park, and K.-T. Kim, "Improved classification performance using ISAR images and trace transform," *IEEE Trans. Aerosp. Electron. Syst.*, vol. 53, no. 2, pp. 950–965, Apr. 2017.
[6] T. Thayaparan, S. Abrol, E. Riseborough, L. Stankovic, D. Lamothe, and G. Duff, "Analysis of radar micro-Doppler signatures from experimental helicopter and human data," *IET Radar, Sonar Navigat.*, vol. 1, no. 4, pp. 289–299, Aug. 2007.
[7] V. C. Chen, "Analysis and interpretation of micro-Doppler signatures," in *The Micro-Doppler Effect in Radar*. Norwood, MA, USA: Artech House, 2011.
[8] S.-H. Yoon, B. Kim, and Y.-S. Kim, "Helicopter classification using time-frequency analysis," *Electron. Lett.*, vol. 36, no. 22, pp. 1871–1872, Oct. 2000.
[9] J. Martin and B. Mulgrew, "Analysis of the theoretical radar return signal form aircraft propeller blades," in *Proc. IEEE Int. Conf. Radar*, May 1990, pp. 569–572.
[10] A. Cilliers and W. A. J. Nel, "Helicopter parameter extraction using joint time-frequency and tomographic techniques," presented at the Int. Conf. Radar, Adelaide, SA, Australia, Sep. 5, 2008.
[11] G. Fliss, "Tomographic radar imaging of rotating structures," presented at the Meeting Synth. Aperture Radar, Los Angeles, CA, USA, Jan. 21, 1992.
[12] F. Zhang, G. Bi, and Y. Qiu Chen, "Tomography time-frequency transform," *IEEE Trans. Signal Process.*, vol. 50, no. 6, pp. 1289–1297, Jun. 2002.
[13] A. Xiaofeng, Z. Xiaohai, Y. Jianhua, L. Jin, and L. Yongzhen, "Feature extraction of rotating target based on bistatic micro-Doppler analysis," presented at the IEEE CIE Int. Conf. Radar, Chengdu, China, Oct. 27, 2011.
[14] C. Rotander and H. V. Sydow, "Classification of helicopters by the L/N quotient," presented at the Radar Syst., Edinburgh, U.K., Oct. 16, 1997.
[15] P. Setlur, F. Ahmad, and M. Amin, "Helicopter radar return analysis: Estimation and blade number selection," *Signal Process.*, vol. 91, no. 6, pp. 1409–1424, Jun. 2011.
[16] P. Addabbo, C. Clemente, and S. L. Ullo, "Fourier independent component analysis of radar micro-Doppler features," in *Proc. IEEE Int. Workshop Metrology for Aerosp. (MetroAeroSpace)*, Jun. 2017, pp. 45–49.

[17] T. M. Cover and J. A. Thomas, "Entropy, relative entropy, and mutual information," in *Elements of Information Theory*. Hoboken, NJ, USA: Wiley, 1991.
[18] A. Hyvärinen and J. Karhunen, "Information theory," in *Independent Component Analysis*. Hoboken, NJ, USA: Wiley, 2001.
[19] E. Bingham and A. Hyvärinen, "A fast fixed-point algorithm for independent component analysis of complex valued signals," *Int. J. Neural Syst.*, vol. 10, no. 1, pp. 1–8, Feb. 2000.
[20] M. H. DeGroot, "Random variables and distributions," in *Probability and Statistics*. London, U.K.: Pearson, 2011.
[21] V. Laparra, G. Camps-Valls, and J. Malo, "Iterative Gaussianization: From ICA to random rotations," *IEEE Trans. Neural Netw.*, vol. 22, no. 4, pp. 537–549, Apr. 2011.
[22] S. Qien, "Short-time Fourier transform," in *Introduction to Time-Frequency and Wavelet Transforms*. Upper Saddle River, NJ, USA: Prentice-Hall, 2001.

INO CHOI received the B.S. and M.S. degrees in electronics engineering from Pukyong National University, Busan, South Korea, in 2012 and 2014, respectively, and the Ph.D. degree from the Pohang University of Science and Technology (POSTECH). In 2010, he joined the Agency for Defense Development, where he is currently a Senior Researcher. He has been a recipient of the Best Paper Award from the Korea Institute of Electromagnetic Engineering and Science (KIEES). His current research interests include micro-Doppler analysis, radar signal processing, automotive target recognition, and the calibration of polarimetric SAR.

KI-BONG KANG received the B.S. and M.S. degrees in electronics engineering from Pukyong National University, Busan, South Korea, in 2015 and 2017, respectively. He is currently pursuing the Ph.D. degree with the Radar and Electomagnetics Signal (REMS) Processing Laboratory, Pohang University of Science and Technology (POSTECH). His current research interests include micro-Doppler analysis, automotive target detection, radar signal processing, and automotive radar signal processing.

JOO-HO JUNG received the B.S. degree from Korea Air Force Academy, Cheongju, South Korea, in 1991, and the M.S. and Ph.D. degrees in electronics engineering from the Pohang University of Science and Technology (POSTECH), Pohang, South Korea, in 1998 and 2007, respectively. From 2008 to 2012, he was a Lieutenant Colonel in charge of planning national defense Research and Development with Defense Acquisition Program Administration, Seoul, South Korea. In 2012, he joined the Faculty of the Department of Electrical Engineering, POSTECH, where he is currently a Research Associate Professor. His research interests include radar target recognition, radar signal processing, and electromagnetic analysis on the wind farm by various military radars.

SANG-HONG PARK received the B.S., M.S., and Ph.D. degrees in electronics engineering from the Pohang University of Science and Technology (POSTECH), Pohang, South Korea, in 2004, 2007, and 2010, respectively. In 2010, he was a Brain Korea 21 Postdoctoral Fellow of the Electromagnetic Technology Laboratory, POSTECH. In 2010, he joined the Faculty of the Department of Electronics Engineering, Pukyong National University, Busan, South Korea, where he is currently an Associate Professor. His research interests include radar target imaging and recognition, radar signal processing, target motion compensation, and radar cross-section prediction.